ÅNGPANNEFÖRENINGENS FORSKNINGSSTIFTELSE

**Forskningsanslag**

# Biosynthesis of the High-value Plant Secondary Metabolites in Yeast

Final Report

October 2019

**Summary**

Plant natural products, such as flavonoids and alkaloids, are widely used as food and feed additives, dietary supplements, nutraceuticals, and pharmaceutical drugs. However, Isolation of valuable plant secondary metabolites from native sources is frequently limited by low abundance and environmental variation while total chemical synthesis of what are often complex structures is typically commercially infeasible. Reconstruction of biosynthetic pathway in heterologous microorganisms offers significant promise for a scalable means to provide sufficient quantities of a desired products while using inexpensive renewable resources. The aromatic amino acid (AAA) biosynthesis pathway is one of the core metabolic pathways that lead to the production of many of these specialty compounds. AAAs act as the primary substrates for the biosynthesis of a wide range of commercially relevant natural products, such as flavonoids and alkaloids, which collectively represent a multi-billion-dollar market value. Therefore, the objective of this project is to develop the yeast *Saccharomyces cerevisiae* for efficient provision of aromatic amino acids for production of alkaloids and flavonoids from renewable feedstocks such as glucose. Here we rewire the central carbon metabolism in yeast such that it efficiently provides E4P and channels more flux through the AAA biosynthesis pathway. In doing so, we can substantially increase the production of AAAs and their derivatives. The contribution of AAA pools toward potential downstream use is evaluated by the formation of *para*-coumaric acid (also called *p*-hydroxycinnamic acid, *p*-HCA). Furthermore, the developed platform cell factories have been evaluated for production of resveratrol, an industrially interesting aromatic chemical.

**Outcomes through the project**

Scientific publications

1. Liu Q.L., Yu T., Campbell K., Nielsen J., **Chen Y**. (2018) Modular pathway rewiring of yeast for amino acid production. *Methods in Enzymology. 608*:265-272.
2. Liu Q.L., Yu T., Li X.W., Chen Y., Campbell K., Nielsen J., **Chen Y**. (2019) Rewiring carbon metabolism in yeast for high level production of aromatic chemicals. *Nature Communications*.  In press.

Conference presentations

1. **Chen Y**. Metabolic engineering of Saccharomyces cerevisiae for high level production of aromatic chemicals (Oral presentation). *Biochemical and Molecular Engineering XXI, July 14-18, 2019. Mont Tremblant, Quebec, Canada*.

Patent applications

1. **Chen Y**. Liu Q.L., Nielsen J. Utilization of phosphoketolase for production of aromatic amino acid derived products. *patent application*.

**Results**

## 1. Dynamic control strategy to increase p-coumaric acid production

Previously, we have proven that introduction of the phosphoketolase (PHK) pathway is an effective approach to increase the metabolic flux of AAAs biosynthesis and subsequently elevate levels of p-coumaric acid (p-HCA) being produced. We next combined this strategy with an enhanced supply of phenylalanine and tyrosine (ePhe and eTyr, via alleviation of bottlenecks in the AAA biosynthesis pathway) for *p*-HCA production (Fig. 1a). Expression of the PHK pathway genes, *Bbxfpk* and *Ckpta*, under the control of the constitutive strong promoters *TDH3p* and *tHXT7p* in strain QL21, together with the *GPP1* deletion resulted in a *p*-HCA titer of 1802.9 mg l$^{-1}$ (strain QL35), representing a 10% increase compared with strain QL21 (Fig. 1b). However, this increase was less pronounced than the *PAL* branch base strains, which demonstrated more than 40% enhancements upon the same introduction of *GPP1* deletion and PHK pathway, suggesting that downstream flux for converting AAA substrates to *p*-HCA was in some way limited. Additionally, a significant decrease in cell growth was observed accompanied by the increased *p*-HCA production for strain QL35 (Fig. 2). Such impairment in cell growth may indicate that rewiring carbon distribution by phosphoketolase expression leads to an insufficient supply of carbon needed for the generation of biomass.
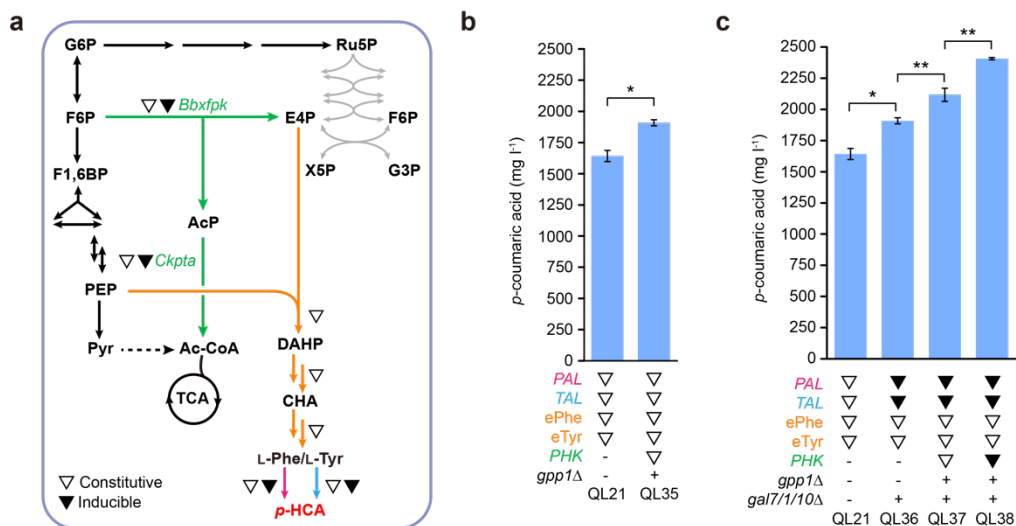


**Fig. 1 Employment of a combinatorial strategy to increase the production of *p*-HCA.** (a) Schematic overview of the metabolic pathway for *p*-HCA production with an improved supply of precursor E4P and dynamic control over the relevant biosynthetic genes, as indicated by triangle symbols: Open triangles indicate the use of constitutive strong promoters to control gene expression, while filled triangles indicate the use of galactose-inducible promoters. See Fig. 1 legend regarding abbreviations of metabolites and Fig. 3 legend for gene details. (b) Integration of the PHK pathway with combined ePhe-*PAL* and eTyr-*TAL* branches leads to increased *p*-HCA production. eTyr refers to enhanced tyrosine biosynthesis mediated through the beneficial effect of *MtPDH1*. (c) Dynamic control of biosynthetic genes via use of the *GAL*-controlled expression system significantly increases *p*-HCA production. Cells were grown in defined minimal medium with 6 tablets of FeedBeads as the sole carbon source and 1% galactose as the inducer when required. Cultures were sampled after 96 h of growth for *p*-HCA detection. Statistical analysis was performed using Student's t test (one-tailed; two-

sample unequal variance; *p* < 0.05, **p* < 0.01, ***p* < 0.001). All data represent the mean ± SD of biological triplicates.
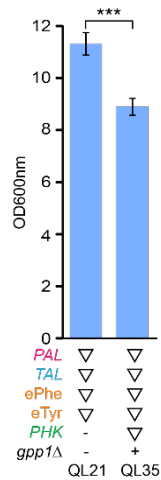


**Fig. 2. Increased *p*-HCA production via phosphoketolase (PHK) pathway expression leads to decreased cell biomass.** Open triangles indicate using constitutive strong promoters to control gene expression. Cells were grown in defined minimal medium with 6 tablets of FeedBeads as the sole carbon source, and cultures were sampled after 96 h of growth for optical density evaluation. Statistical analysis was performed using one-tailed Student's t test (one-tailed; two-sample unequal variance; *p* < 0.05, **p* < 0.01, ***p* < 0.001). All data represent the mean ± SD of biological triplicates.

To fine tune the expression levels so far attained, we next employed dynamic control using the well characterized *GAL*p expression system to control the expression of heterologous genes that divert AAAs towards *p*-HCA synthesis (Fig. 1a). *GAL* expression is only responsive to galactose exposure without glucose repression, which can in turn facilitate cell growth under excess glucose conditions. The expression of genes under *GAL* promoter control has also shown to be much stronger when compared to normally employed strong constitutive promoters such as *TEF1p* and *TDH3p*. Therefore, the *GALp*-controlled expression system was firstly tested for both the *PAL* and *TAL* branch genes. To enable this, the structural genes *GAL7/1/10* were deleted in QL21 to confer galactose as a gratuitous inducer, with *GAL1, GAL2* and *GAL7* promoters being used to control expression of *AtPHA2, AtC4H* and *FjTAL*. The resultant strain QL36 produced 10% higher of *p*-HCA than that of QL21 (Fig. 1c), which indeed proved that the *GAL* promoters were more suitable in this instance than the constitutive *TEF1* and *TDH3* promoters. Consequently, we then examined phosphoketolase expression in QL36 either under the control of constitutive promoter or galactose-regulated promoter systems. Strain QL37 with the constitutive promoter control system produced *p*-HCA at a level of 2116.7 mg l$^{-1}$, whereas incorporation of the galactose-induced expression cassette led to a more significant (*p*<0.01) increase in *p*-HCA titer to 2406.1 mg l$^{-1}$ (strain QL38), a 33% increase compared with QL36 (Fig.1c). Moreover, when using this background (strain QL36), inducible expression of phosphoketolase showed less significant effects on cell growth (data not shown).

2. Balancing the availability of PEP and E4P

Based on the optimized betaxanthin biosensor, we selected the strain QL45 that only had the PHK pathway and feedback insensitive Aro4$^{K229L}$, as the host for promoter library screening. We then co-transformed 30 promoter cassettes and a triple gRNA vector into this strain and selected transformants

using glucose as the sole carbon source. From these transformants, eight colonies displaying enhanced color intensity were selected and subjected to identification of promoter substitutions (Table 1). These strains were then characterized for cell growth and betaxanthin color intensity (Fig. 3). Of these promoter substitutions, the two most optimal combinations were as follows: first, the replacement of *PFK1*, *PFK2* and *PYK1* native promoters with *SET3*p, *CDC24*p and *ALD5*p; second, the substitution of *PFK1*, *PFK2* and *PYK1* native promoters with *ILV3p*, *CDC24p* and *LYS20p*, respectively. Reconstruction of these genes with these promoter replacements in the high producer strain QL38 resulted in strains QL50 and QL56, containing the first and second combination of replacement promoters respectively (Fig. 4b). Both strains rendered a further increase in the titer of *p*-HCA with the best performing strain, QL50, producing 2680.2 mg l$^{-1}$ of *p*-HCA, a 11% increase compared with QL38.

**Table 1. Promoter substitution profiles of identified yeast strains.**

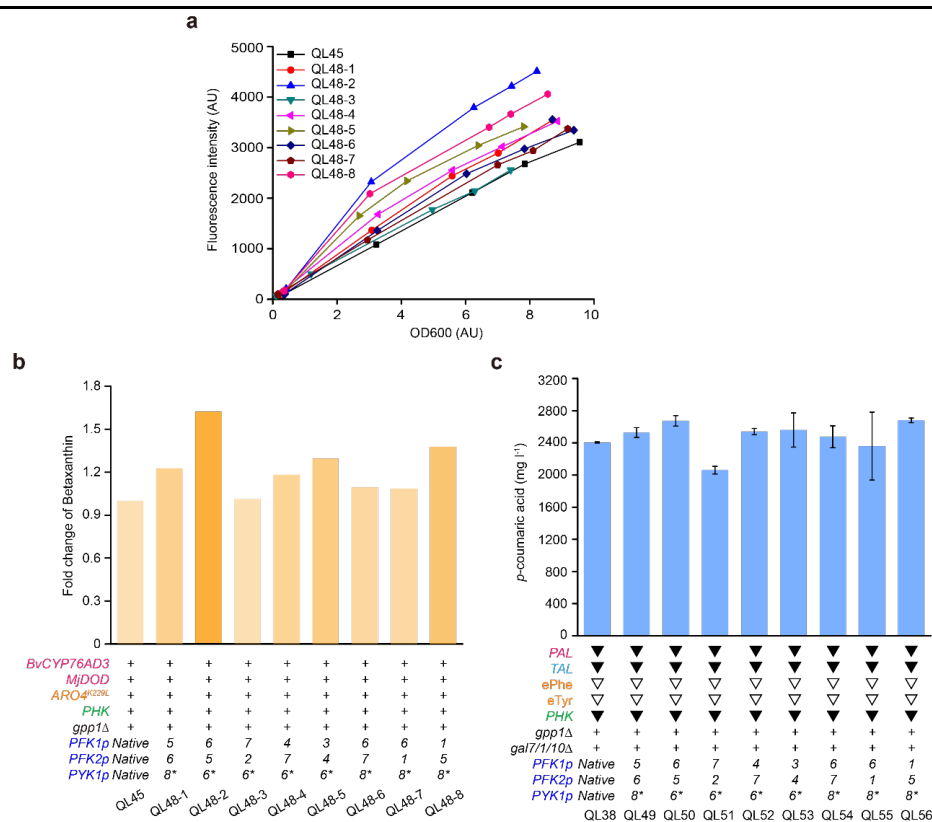| Betaxanthin strains (QL48-#) | *PFK1* upstream | *PFK2* upstream | *PYK1* upstream | Corresponding *p*-HCA strains |
|---|---|---|---|---|
| 1 | *CDC24p* | *SET3p* | *LYS20p* | QL49 |
| 2 | *SET3p* | *CDC24p* | *ALD5p* | QL50 |
| 3 | *IDP1p* | *ADH3p* | *ALD5p* | QL51 |
| 4 | *BAT1p* | *IDP1p* | *ALD5p* | QL52 |
| 5 | *VMA6p* | *BAT1p* | *ALD5p* | QL53 |
| 6 | *SET3p* | *IDP1p* | *LYS20p* | QL54 |
| 7 | *SET3p* | *ILV3p* | *LYS20p* | QL55 |
| 8 | *ILV3p* | *CDC24p* | *LYS20p* | QL56 |

**Fig. 3. Evaluation of the promoter replaced strains based on betaxanthin screening.** (**a**) Cell growth and betaxanthin accumulation in selected promoter-replaced strains. Cells were grown in defined minimal medium with 6 tablets of FeedBeads as the sole carbon source. All data represent the mean of biological triplicates. (**b**) Relative accumulation level of betaxanthin in selected promoter-replaced strains compared with strain QL45 as the reference. The values denote the normalized fold change of betaxanthin accumulation per cell mass increase. The color change in bars reflects increase in betaxanthin formation. Exact promoters in selected promoter-replaced strains are indicated as corresponding numbers listed in Supplementary Table 2. (**c**) Reconstitution of the promoter replacement in engineered *p*-HCA producer (QL38) background. Open triangles indicate using constitutive strong promoters to control gene expression, while filled triangles indicate using galactose-induced promoters. Cells were grown in defined minimal medium with 6 tablets of FeedBeads as the sole carbon source and 1% galactose as inducer. All data represent the mean of biological triplicates.

Although deletion of the *GAL7/1/10* gene cluster strains were not able to metabolize galactose, these strains still require a low concentration of galactose for induction of the *PAL*, *TAL* and PHK pathway genes transcribed by *GAL* promoters. To avoid the use of galactose, we deleted the *GAL80* gene (Fig. 4c), allowing for the induction of galactose regulated genes upon the release of carbon repression such as by glucose. This approach has been reported to work under similar conditions to ours under glucose-limited fed-batch fermentation conditions without the addition of galactose.
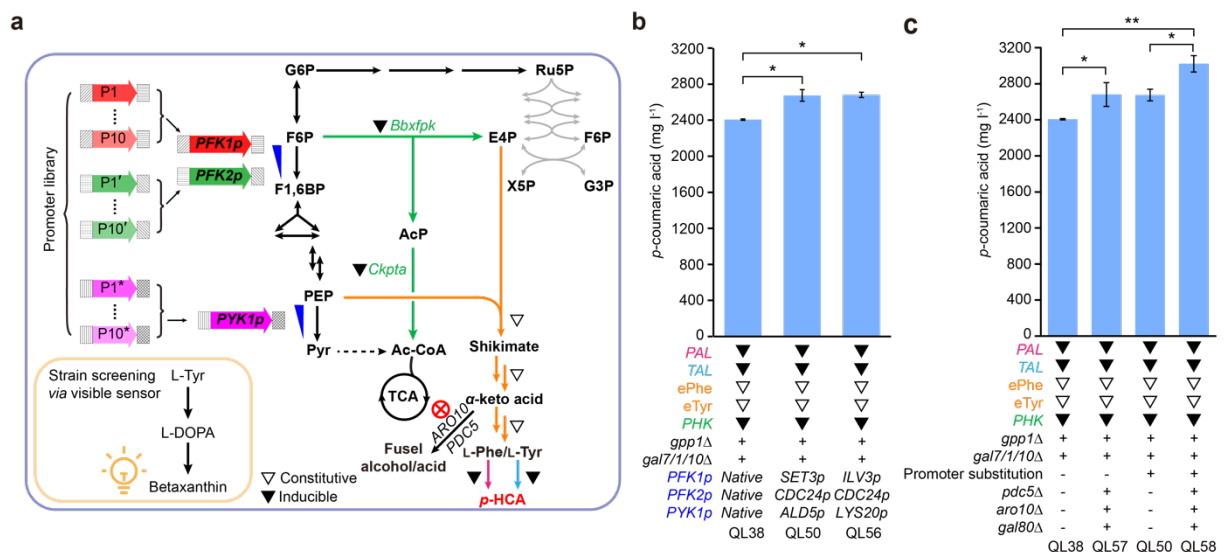


**Fig. 4 Optimization of carbon distribution increases *p*-HCA production.** (**a**) Schematic illustration of carbon redistribution between glycolysis and the AAA biosynthesis pathway through a promoter library screening approach. A promoter library was created to replace the original promoters of *PFK1*, *PFK2*, and *PYK1*, which encode phosphofructokinase and pyruvate kinase respectively at key nodes between glycolysis and the AAA biosynthesis pathway. This promoter library was transformed into a yeast strain harboring the PHK pathway alongside the upregulated shikimate pathway, with resulting strain screened using a L-Tyr-derived pathway that indicated increased tyrosine production via the formation of the yellow pigment betaxanthin. Selected promoters exhibiting enhanced color intensity are listed in Supplementary Table 2. Furthermore, AAA degradation pathway was eliminated by deleting the corresponding genes (marked with a red cross) in the final strains. Open triangles indicate

the use of constitutive strong promoters for controlling gene expression, while filled triangles indicate the use of galactose-inducible promoters. (**b**) Simultaneous optimization of the promoters of *PFK1*, *PFK2*, and *PYK1* improves *p*-HCA production. (**c**) Removing the AAA degradation pathway further enhances p-HCA titers. Deletion of *GAL80* was additionally introduced to enable the induction of *GAL* promoters without the addition of galactose. For shake flask cultivation, cells were grown in defined minimal medium with 6 tablets of FeedBeads as the sole carbon source and 1% galactose as the inducer when required. For strains with the deletion of *GAL80*, no galactose was supplemented. Cultures were sampled after 96 h of growth for *p*-HCA detection. Statistical analysis was performed using Student's t test (one-tailed; two-sample unequal variance; *$p < 0.05$, **$p < 0.01$, ***$p < 0.001$). All data represent the mean ± SD of biological triplicates.

As previously reported, increased fluxes in the AAA biosynthesis pathway led to a significant increase in fusel aromatic compounds with the deletion of *ARO10* and *PDC5* effectively blocking this route for AAA degradations. Indeed, phenylethanol, *p*-hydroxyphenylethanol and the related acids were found to be accumulated in strain QL38, while knocking out both *ARO10* and *PDC5* (Fig. 5a) significantly reduced these by-products (data not shown). Interestingly, unlike our earlier attempt to remove the AAA degradation pathway, the introduction of these two deletions at this stage of our work, led to less significant negative impact on cell growth. Consequently, the double deletion was able to further enhance the production of *p*-HCA by 11% (strain QL57, Fig. 4c). These effects were similarly seen in the strain with promoter replacements (QL50). Interestingly, the accumulation of by-products such as phenylethanol and phenylacetate was further increased in strain QL50, compared with that detected in QL38 (data not shown), indicating that the carbon flux through the AAA biosynthesis pathway had been further increased in QL50. As a result, the double deletions in the promoter substituted strain led to further enhanced *p*-HCA production, reaching a titer of 3021.2 mg l$^{-1}$ in the shake flask cultivation (strain QL58, Fig. 4c), a 26% improvement compared with QL38. To the best our knowledge, this is the highest reported titer achieved for aromatic compounds in yeast shake flask cultivations, with a yield of 151.1 mg g$^{-1}$ glucose corresponding to ~43 % of the maximum theoretical yield possible (this being 0.3494 g/g).

3. High level production of p-coumaric acid

The production of *p*-HCA in our best performing strain (QL58) was almost doubled comparing to that of QL158, confirming that the PHK pathway-based carbon rewiring strategies we employed could effectively divert more carbon flux towards AAA biosynthesis and *p*-HCA production. In subsequent evaluation of these strains under glucose-limited fed-batch fermentation conditions, QL158 only produced 5.1 g l$^{-1}$ of *p*-HCA, while QL58 produced *p*-HCA at a titer of 10.4 g l$^{-1}$ (Fig. 5a and 5b). This was consistent with a significant increase ($p<0.05$) in the rate of *p*-HCA production, which almost doubled in QL58 in comparison with QL158 (Table 2). Furthermore, metabolic flux analysis showed that the carbon flux was redistributed among glycolysis, PPP and AAA biosynthesis pathway in QL58 with the PHK pathway-based carbon rewiring strategies, compared with that in QL158 lacking these carbon rewiring strategies (Fig. 5c). These results clearly show that the glycolytic flux was diverted towards

E4P formation and AAA biosynthesis, and by redistributing this flux, it was possible to achieve about two-fold enhancement of carbon flux towards E4P and AAA biosynthesis in QL58 (Fig. 5c).

As diploid strains typically perform better than the corresponding haploid strains, we further constructed a diploid strain by switching the mating-type of QL58, and then mating the resulting strain with QL58 producing a diploid strain with identical chromosome pairs. The resulting diploid strain (QL60) performed slightly better than QL58, with a titer of 3098.7 mg l$^{-1}$ and a yield of 154.9 mg g$^{-1}$ glucose in the shake flask cultivation. Finally, we evaluated the performance of the diploid strain QL60, under glucose-limited fed-batch fermentation conditions, wherein *p*-HCA production reached 12.5 g l$^{-1}$, the highest titer reported in literature for aromatics produced in yeast up to date (Fig. 5a and 5b). Additionally, these high titers resulted in crystallization of *p*-HCA in the culture broth (Fig. 5d).
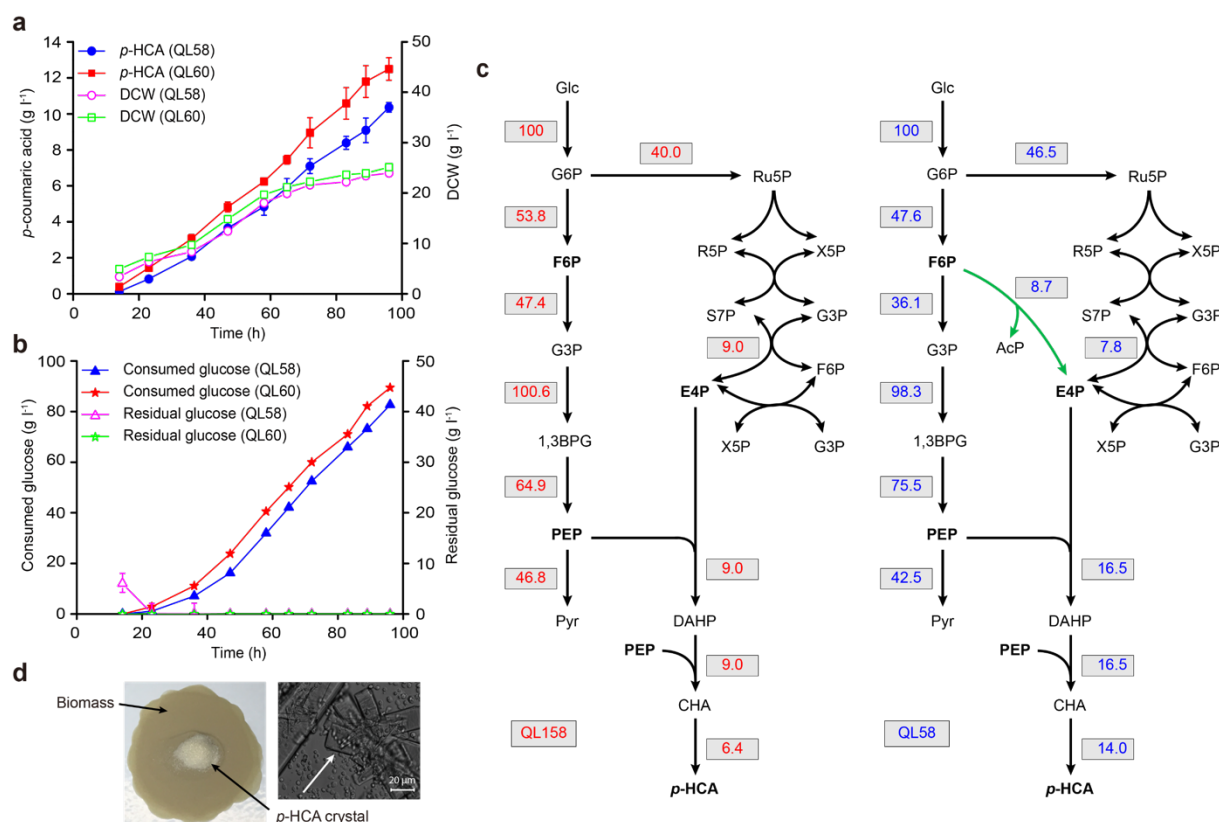


**Fig. 5 High-level production of *p*-HCA.** (a) Fed-batch fermentation of strain QL58 and the corresponding diploid strain QL60 under glucose limited conditions over time. *p*-HCA titer (filled symbols) and cell mass (open symbols) are shown for each strain. (b) Glucose consumption profile (filled symbols) and time course of residual glucose (open symbols) during the same fed-batch fermentation for each strain. The data represent the mean ± SD of biological duplicates. (c) Predicated metabolic flux distributions via flux balance analysis (FBA) in the engineered medium-level *p*-HCA producer QL158 (left, without carbon rewiring strategy) and high-level *p*-HCA producer QL58 (right, with carbon rewiring strategy). Based on FBA, the fluxes to the different products were represented relative to the uptake of 100 mmol of glucose. The PHK pathway, the non-native E4P-forming biosynthetic pathway, is highlighted in green. 1,3BPG, 1,3-biphosphoglycerate; and see Fig. 1 legend regarding abbreviations of other metabolites. (d) Observed *p*-HCA crystals on filter membrane (left panel) and under microscope (right panel, scale bar = 20 μm). Crystals of *p*-HCA were formed as a result of its high-level production and relatively low solubility in the fed-batch fermentation broth.

**Table 2. Physiological parameters of engineered *p*-HCA producing strains[a]**

| Parameter | QL158 | QL58 |
|---|---|---|
| $\mu$ (max) (h$^{-1}$) | 0.038 ± 0.0004 | 0.029 ± 0.001 |
| Y(x/s) (g g$^{-1}$) | 0.326 ± 0.014 | 0.323 ± 0.009 |
| q(Glucose) (mmol gDCW$^{-1}$ h$^{-1}$) | -0.562 ± 0.025 | -0.479 ± 0.004 |
| q(Glycerol) (mmol gDCW$^{-1}$ h$^{-1}$) | 0.061 ± 0.008 | N.D. |
| q(*p*-coumaric acid) (mmol gDCW$^{-1}$ h$^{-1}$) | 0.036 ± 0.0003 | 0.0672 ± 0.005 |
| q(Biomass) (mmol gDCW$^{-1}$ h$^{-1}$) | 1.559 ± 0.014 | 1.175 ± 0.040 |
| q(CO$_2$) (mmol gDCW$^{-1}$ h$^{-1}$) | 1.469 ± 0.019 | 1.140 ± 0.071 |
| q(O$_2$) (mmol gDCW$^{-1}$ h$^{-1}$) | -1.494 ± 0.012 | -1.141 ± 0.055 |
| Carbon balance | 105 ± 5% | 102 ± 3% |

[a] Data represent the mean ± SD of biological duplicates. N.D. not detected.

4. Production of other important aromatic compounds

To discuss and showcase the utility of our optimized strains in the production of other value-added aromatic compounds, we engineered and evaluated the resveratrol biosynthetic pathway in our engineered strains (Fig. 6a). Introduction of *Arabidopsis thaliana* 4-coumarate-CoA ligase 1 (*At4CL1*) and *Vitis vinifera* stilbene synthase (*VvSTS*) into strain QL58 produced only 32.1 mg l$^{-1}$ of resveratrol. However, approximately 2500 mg l$^{-1}$ *p*-HCA accumulated in this strain (QL375, Fig. 6b), indicating that another precursor, malonyl-CoA, was limiting. Indeed, by further combination of the deregulated mutant *ACC1$^{S659A, S1157A}$* resveratrol production was significantly ($p<0.001$) increased, reaching a titer of 263.4 mg l$^{-1}$ (QL379, Fig. 6b), which is comparable with the highest level reported for production of this compound in shake-flask cultivation of yeast cells. It is also interesting to be noted that in this strain, almost 2 g l$^{-1}$ *p*-HCA was found to remain, again demonstrating that the strategies we employed were efficient at enhancing carbon flux through the AAA biosynthesis pathway.
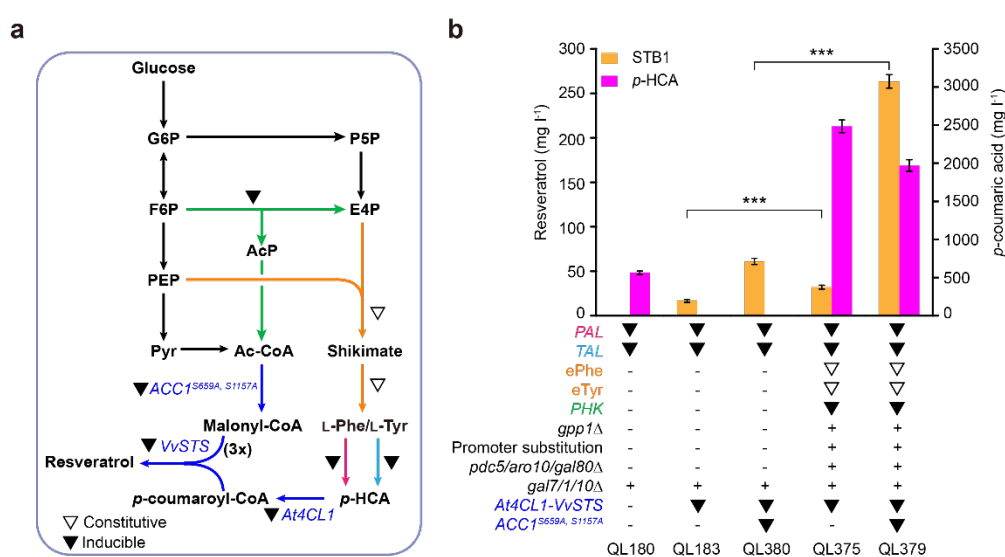


**Fig. 6. Enabling higher resveratrol production by engineered *p*-HCA biosynthesis.** (a) Schematic illustration of resveratrol biosynthetic pathway in the context of enhanced supply of precursor *p*-HCA.

The resveratrol biosynthetic pathway consists of *Arabidopsis thaliana* 4-coumarate-CoA ligase 1 (*At4CL1*) and *Vitis vinifera* stilbene synthase (*VvSTS*); the deregulated mutant $ACC1^{S659A,\ S1157A}$ was overexpressed to increase the supply of another precursor malonyl-CoA. Open triangles indicate use of constitutive strong promoters to control gene expression, while filled triangles indicate use of galactose-induced promoters. (**b**) Resveratrol and *p*-HCA titers obtained with engineered strains. Cells were grown in defined minimal medium with 6 tablets of FeedBeads as the sole carbon source and 1% galactose as inducer when required. For strains with deletion of GAL80, no galactose was supplemented. Cultures were sampled after 96 h of growth for resveratrol and *p*-HCA detection. Statistical analysis was performed using Student's t test (one-tailed; two-sample unequal variance; \**p* < 0.05, \*\**p* < 0.01, \*\*\**p* < 0.001). All data represent the mean of n = 3 biologically independent samples and error bars show standard deviation. Source data of Supplementary Figure 19b are provided as a source data file.

## Conclusions

One of the main bottlenecks in the production of aromatic chemicals occurs in the shikimate and AAA biosynthesis pathway. AAAs are less abundant than other amino acids inside the cell, moreover the flux towards their biosynthesis is highly regulated. In particular, the availability of E4P is severely limited in many microorganisms, resulting in a significant constraint on entry flux for AAA biosynthesis. This limitation thus represents a major challenge for producing industrially relevant aromatic chemicals at high levels. Through this project, we have successfully rewired yeast central carbon metabolism to enhance flux through the AAA biosynthesis pathway and support biosynthesis of the target molecule, *p*-HCA. This was accomplished by systematically engineering the AAA biosynthesis pathway, introducing a phosphoketalose (EC 4.1.2.22)-based pathway to divert glycolytic flux towards the formation of E4P, and further optimizing the carbon distribution between glycolysis and the AAA biosynthesis pathway through replacing the promoters of several important genes at key nodes between these two pathways, to balance the availability of the AAA precursors PEP and E4P. These strategies resulted in a maximum *p*-coumaric acid titer of 12.5 g l$^{-1}$ and a maximum yield on glucose of 154.9 mg g$^{-1}$, the highest reported titer and yield for aromatic chemical production in yeast. Although further optimization may well be required, we are confident the carbon rewiring strategies presented here provide a promising platform for production of many other flavonoids and alkaloids derived from phenylalanine and tyrosine.